SPi | Journal Code: S I A | Article ID: 5 7 5 9 | Dispatch: 10.03.15 | CE: | No. of Pages: 10 | ME:

Research article

SURFACE and INTERFACE ANALYSIS

Received: 27 August 2014 Revised: 24 February 2015 Accepted: 24 February 2015 Published online in Wiley Online Library

(wileyonlinelibrary.com) DOI 10.1002/sia.5759

Surface composition of PdCuAu ternary alloys: a combined LEIS and XPS study

Ana M. Tarditi,[a] Carolina Imhoff,[a] James B. Miller[b] and Laura Cornaglia[a]*

PdCuAu ternary alloy samples with different composition were synthesized on top of ZrO_2-modified porous stainless steel disks by the sequential electroless deposition technique. The structure, morphology and bulk composition of the samples were characterized by X-ray diffraction (XRD), scanning electron microscopy and energy dispersive X-ray spectroscopy (EDX). Complete alloy formation with a pure fcc phase for the $Pd_{71}Cu_{26}Au_3$, $Pd_{70}Cu_{25}Au_5$ and $Pd_{67}Cu_{24}Au_9$ samples and a bcc structure for the $Pd_{62}Cu_{36}Au_2$ and $Pd_{60}Cu_{37}Au_3$ samples were obtained upon annealing at 500 °C for 120 h as revealed by XRD. A combination of low-energy ion scattering (LEIS) and X-ray photoelectron spectroscopy (XPS) was used to investigate the surface properties of the PdCuAu alloys. XPS results confirmed alloy formation under the annealing conditions. XPS analysis also revealed that the near-surface regions of the alloys became enriched in Pd with respect to the bulk composition determined by EDX. In contrast, LEIS and angle-resolved XPS analyses showed that the top-most surface layers in all samples were copper-rich compared with the bulk composition. This high Cu surface concentration could impart resistance to bulk sulfide formation to the PdCuAu alloy membranes. Copyright © 2015 John Wiley & Sons, Ltd.

Keywords: pdCuAu ternary alloys; surface segregation; LEIS and XPS measurements

Introduction

Palladium-based binary and ternary alloys are important materials for applications in catalysis and as membranes for hydrogen purification. In these processes, reaction and hydrogen dissociation takes place at the alloy surface. The surface composition of an alloy usually differs from that of the bulk; therefore, detailed information about the surface compositions of alloys plays an important role in the interpretation of physical and chemical properties that are relevant to their performance as membranes and catalysts. For palladium-based hydrogen separation membranes, it is known that both surface and bulk compositions influence alloy permeability. Hence, a deeper understanding of the relationship between its surface properties and hydrogen permeability may lead to the development of new materials with improved permeation performance.

Dense palladium membranes are attractive for hydrogen purification as a result of their efficiency and high selectivity toward hydrogen. However, pure Pd undergoes a hydride phase transition upon hydrogen absorption at temperatures below 300 °C,[1] which causes irreversible embrittlement of the Pd film. Furthermore, Pd can be irreversibly poisoned by sulfur compounds and other feedstock components, which can cause deterioration of membrane performance.[2] It is well known that alloying Pd with other metals such as Ag, Cu and Au can overcome these drawbacks and even improve hydrogen permeability.[3] PdCu and PdAu can have high sulfur-poisoning resistance.[4–6] PdCu alloys with fcc structure are tolerant to H_2S exposure, but they have relatively low base (in clean H_2) permeabilities. On the other hand, PdCu alloys with bcc structure display high permeabilities but poor H_2S tolerance. The incorporation of a third component, such as Au, has the potential to increase the H_2 permeability of the fcc PdCu phase, while maintaining or even imparting additional H_2S tolerance.

Surface studies carried out by Miller *et al.*[7] on PdCu alloys have shown that the top atomic layer is rich in Cu as determined by means of low-energy ion scattering (LEIS), whereas the near-surface region determined from X-ray photoelectron spectroscopy (XPS; ~7 atomic layers) is rich in Pd.[7] This difference was attributed to the depletion of Cu in the atomic layers immediately below the top. These data were consistent with those reported by Loboda-Cackovic *et al.*[8] using Auger electron spectroscopy (AES) and temperature-programmed desorption (TPD) of CO. Brongersma and coworkers[9] reported the segregation of the majority component for the Cu_3Pd system, as revealed by LEIS, in agreement with theoretical predictions.[10] On the other hand, in LEIS experiments, a composition of about 90% of Au in the first layer and less than 10% in the second layer was observed for a $Cu_{50}Au_{50}$ alloy,[11] which indicated an oscillatory composition profile as shown by Tersoff.[12] For the PdAu system, several studies have reported differences between the surface and the bulk composition,[13,14] showing a higher Au concentration on the surface. In some cases, a slight enrichment of Au was found through Auger transition analysis and a more pronounced gold enrichment was determined by LEIS experiments.[14] Goodman and coworkers[14] attributed this discrepancy to the difference synthesis procedure of the samples.

Compared with several studies of surface segregation in binary systems, fewer publications have reported surface segregation in multi-component alloys.[15,16] For PdCuAg alloys, a Cu and Ag cosegregation to the near-surface region was observed as well as

* *Correspondence to: L. Cornaglia, Instituto de Investigaciones en Catálisis y Petroquímica (FIQ, UNL-CONICET), Santiago del Estero 2829, 3000 Santa Fe, Argentina.*
E-mail: lmcornag@fiq.unl.edu.ar

a *Instituto de Investigaciones en Catálisis y Petroquímica, (FIQ, UNL-CONICET), Santiago del Estero 2829, 3000 Santa Fe, Argentina*

b *Department of Chemical Engineering, Carnegie Mellon University, 5000 Forbes Avenue, 15213 Pittsburgh, PA, USA*

a silver enrichment of the top-most surface region through angle-resolved XPS (ARXPS) and LEIS experiments, respectively.[17]

The present work deals with the synthesis and surface characterization of PdCuAu ternary alloy samples synthesized by the sequential electroless deposition technique on top of porous stainless steel disks. Alloy composition selections were guided by high-throughput studies of S uptake by composition spread alloy film (CSAF) combinatorial libraries[18] conducted at Carnegie Mellon University. Results of the work will be reported separately. Briefly, thin (~100 nm) $Pd_{1-x-y}Cu_xAu_y$ alloy films were codeposited onto compact (~14 × 14 mm^2) Mo substrates by physical vapor deposition methods. Annealed CSAFs were exposed to 100 ppm H_2/H_2S at 400 °C for 24 h and then characterized for S uptake by XPS and energy dispersive X-ray spectroscopy (EDX). The compositions for the present work were chosen from regions that displayed low S uptake and therefore potential for corrosion resistance.

The effect of the annealing time at 500 °C in H_2 on the alloy formation was investigated by X-ray diffraction (XRD) on PdCuAu films synthesized by electroless plating (ELP). The morphology and bulk composition of the as-synthesized samples were analyzed by scanning electron microscopy (SEM)-EDX. A combination of LEIS and XPS measurements were used to investigate the surface compositions in the top-most atomic layer and in the near-surface region, respectively.

Experimental

Sample synthesis

The PdCuAu alloy samples were synthesized on top of porous 316L stainless steel disks (PSSD, 1.27 cm in diameter and thickness of 4 mm, 0.1 μm grade). The supports were purchased from Mott Metallurgical Corporation®. Prior to any plating experiment, supports were cleaned in a basic solution consisting of 0.12 M Na_3PO_4, 12 H_2O, 0.6 M Na_2CO_3 and 1.12 M NaOH. Later, the disks were oxidized at 500 °C for 12 h. To avoid inter-metallic diffusion between the stainless steel elements and the PdCuAu ternary alloy, the supports were modified with ZrO_2 by the dip-coating vacuum-assisted method.[19] Solutions for activation were prepared using tin(II) chloride dehydrate and palladium(II) chloride. The chemical compositions of the activation and plating solutions used were reported elsewhere.[19,20] The activation procedure consisted of first dipping the substrate in the tin chloride solution and then in palladium chloride solution with intermediate rinsing in water between the immersions. After dipping the support in the chloride solution, it was rinsed with a 0.01 M HCl solution to avoid reoxidation of palladium. This cycle was repeated as needed, normally three times. The ELP technique was used to coat the support with a continuous metallic film. Palladium, gold and copper were deposited by sequential electroless deposition. Figure 1 shows the sequence used for the Pd, Cu and Au electroless deposition. For all membranes, palladium was deposited in two steps of 60 min each, followed by a Au deposition. After the Pd and Au depositions, the samples were rinsed with water and dried at 120 °C overnight. The Cu plating was performed on top of the Pd-Au layers, previously activated with $SnCl_2$ and $PdCl_2$. Plating times for Pd, Au and Cu were adjusted to achieve the desired metal composition in all cases. After the electroless deposition of Cu, the samples were immediately immersed in 0.01 M HCl to neutralize any residual plating solution, followed by rinsing with deionized water and ethanol to facilitate drying and prevent oxidation of the copper layer. The sample was then heated up to 500 °C in H_2 at atmospheric pressure (101.32 kPa) in order to form a homogeneous palladium-gold-copper alloy by thermal diffusion. To obtain a higher film thickness, a second set of Pd, Au and Cu layers was applied, followed by a second heat treatment at the same temperature. The nomenclature adopted for the samples was $Pd_xCu_yAu_z$ where x, y and z refer to the atomic bulk composition determined by EDX.

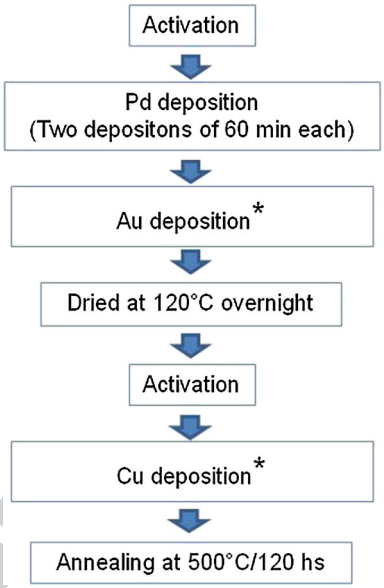

Figure 1. Scheme of the deposition cycle used for the synthesis of the PdCuAu samples studied.

Sample characterization

X-ray diffraction

The phase structure of the samples as a function of annealing time was determined by XRD. The XRD patterns of the films were obtained with an XD-D1 Shimadzu instrument, using CuKα (λ = 1.542 Å) radiation at 30 kV and 40 mA. The scan rate was 1–2 min^{-1} in the range 2θ = 15–90°.

Scanning electron microscopy and energy dispersive X-ray analysis

The outer surface and cross-section images of the samples were obtained using a JEOL scanning electron microscope, model JSM-35 C, equipped with an energy dispersive analytical system.

X-ray photoelectron spectroscopy

XPS analyses were performed in a multi-technique system (SPECS) equipped with a hemispherical PHOIBOS 150 analyzer operating in the fixed analyzer transmission mode. The spectra were obtained using a monochromatic AlKα radiation (hυ = 1486.6 eV) operated at 300 W and 14 kV. The pass energy for the element scan was 30 eV. The working pressure in the analyzing chamber was less than 5×10^{-10} kPa. The XPS analyses were performed on the annealing samples. After preparation, the samples were exposed to ambient conditions and transferred to the load-lock chamber of the spectrometer where they were heated in flowing H_2(5%)/Ar at 400 °C for 10 min. Then, they were transferred to the analysis chamber without air exposure, and the surface characterization was performed.

SURFACE and INTERFACE ANALYSIS

The spectra of Pd 3d, Pd 3p, O 1s, C 1s, Au 4f, Cu 2p and Fe 2p were recorded for each sample. The data treatment was performed with the Casa XPS program (Casa Software Ltd., UK). The peak areas were determined by integration employing a Shirley-type background. Peaks were considered to be a mixture of Gaussian and Lorentzian functions. Sensitivity factors provided by the instrument manufacturer were used for the quantification of composition. The kinetic energies of the Pd $3d_{3/2}$, Cu $2p_{3/2}$ and Au $4f_{7/2}$ signals were 1145, 555 and 1402 eV, respectively, which correspond to mean free paths of about 10–15 Å. Thus, the XPS experiments gave compositional information coming from ca. the first 6 atomic layers.

By varying the takeoff angle between the direction of the escaping photoelectron and the surface plane of the sample, the depth profile distribution within the near-surface region was obtained. Measurements were made at different angles by tilting the sample with respect to the analyzer. For each ARXPS experiment, measurements were performed at six different angles between 0 and 64° with respect to the surface normal. These angles represent integrated XPS analysis depth of ca. 6 and 2 atomic layers, respectively.

XPS depth profile experiments

Depth profile measurements were performed using Ar^+ sputtering. A differentially pumped ion gun was operated at 7×10^{-8} kPa, 3 keV and 300 nA. Under these conditions, sputtering rates of ca. 1.1 nm min^{-1} are produced as estimated by the method reported by Hofmann.[21] Sputtering times up to 70 min were used to probe depths of up to 80 nm. Before sputtering and then at each sputtering step, photoemission spectra for Pd 3d, Cu 2p, Au 4f, O1s and C 1s core levels were recorded; peak areas were determined by integration employing a Shirley-type background. Sensitivity factors provided by the instrument manufacturer were used for quantification of the elements.

LEIS spectroscopy

LEIS analysis, for estimation of top-surface composition, was performed using a differentially pumped ion source IQE 12/38 SPECS, in the multi-technique system (SPECS). The LEIS spectra were taken using 1 keV helium ions at a scattering angle of 50°, with a current density of about 400 nA cm^{-2} (1.5×10^{14} ion cm^{-2} to take a complete experiment) to minimize the potential for surface etching. The primary ion beam was focused onto a 1 mm diameter spot size on the sample. Reference samples to calibrate the LEIS signals and to obtain sensitivity factors were pure Pd, Au and Cu foils. The Pd, Cu and Au reference samples were cleaned under ultrahigh vacuum (UHV) conditions by repeated cycles of argon ion bombardment (3 keV). The cleanliness of the samples was checked by XPS. For the quantitative estimates of the top layer composition, we compared the LEIS peak areas (Gaussian fits) at E/E_0 0.85, 0.78 and 0.89, corresponding to Cu, Pd and Au, respectively.

The surface concentration of an element A in the alloy was determined from the LEIS spectra using Eqn (1):

$$C_A = \frac{I_A}{I_A + f_{A/B}.I_B + f_{A/C}.I_C} \quad (1)$$

where I_A, I_B and I_C are the intensities of the ions scattered at atoms A, B and C with concentrations C_A, C_B and C_C; with $C_A + C_B + C_C = 1$, $f_{A/B}$ and $f_{A/C}$ are the ratios of the peak scattered intensities of the pure metals.

Results and discussion

PdCuAu alloy formation and morphological study

Alloy composition selections were guided by high-throughput studies of S uptake by CSAF combinatorial libraries[18] conducted at Carnegie Mellon University. Annealed CSAFs were exposed to 100 ppm H_2/H_2S at 400 °C for 24 h and then characterized for S uptake by XPS and EDX. Alloy compositions for the present work were chosen from regions that displayed low S uptake and therefore potential for corrosion resistance.

Table 1 summarizes the compositions and thicknesses of the PdCuAu samples synthesized by means of sequential electroless deposition. The desired composition was achieved by modification of the deposition times of Au and Cu, as shown in Fig. 1. As observed in Table 1, the samples studied can be divided into two main groups based on their Cu concentration: the $Pd_{60}Cu_{37}Au_3$ and $Pd_{62}Cu_{36}Au_2$ samples with a higher Cu composition and the $Pd_{70}Cu_{26}Au_4$, $Pd_{67}Cu_{24}Au_9$ and $Pd_{71}Cu_{26}Au_3$ samples with a lower Cu content. T1

XRD patterns of the $Pd_{70}Cu_{26}Au_4$ sample, after the metallic deposition, and then of the annealing in hydrogen at 500 °C for 120 h, are shown in Fig. 2a. After metal deposition, the sample displayed the expected pure component Pd, Au and Cu diffraction patterns. After annealing, a complete fcc alloy formation was observed. No evidence of the bcc crystalline phase or impurities was detected. The diffraction patterns of samples $Pd_{71}Cu_{26}Au_3$ and $Pd_{67}Cu_{24}Au_9$ yielded similar profiles showing the formation of pure fcc alloys (data not shown). In contrast, after annealing at 500 °C for 120 h, the XRD patterns of the $Pd_{60}Cu_{37}Au_3$ and $Pd_{62}Cu_{36}Au_2$ samples indicated the formation of a pure bcc crystal structure (Fig. 2b). It is worth noting that in the XRD patterns, no reflection peaks from Fe, Cr, Ni or Zr were observed. F2

As previously reported,[22] the bcc structure for the PdCu system is stable in a region of intermediate composition at low temperature. Furthermore, it has been reported that the addition of small amounts of gold to the PdCu alloy does not prevent the formation of the bcc phase.[22] In the PdCuAu ternary phase diagram, three structures are thermodynamically stable at 400 °C, a disordered fcc phase, a tetragonal phase and a bcc phase.[22] Bredesen and coworkers[23] reported a complete fcc alloy formation with no evidence of the bcc crystalline phase for $Pd_{71.5}Cu_{27}Au_{1.5}$ and $Pd_{72.1}Cu_{24.7}Au_{3.2}$ alloys synthesized by magnetron sputtering. On the other hand, Coulter *et al.*[24] modeled and fabricated by magnetron sputtering several PdCuAu membranes with different compositions, obtaining a fcc structure in all cases. Guerreiro *et al.*[25] recently prepared several PdCuAu alloys by coelectrodeposition over a large composition range showing fcc phase formation. These latter authors observed shifts in diffraction peak locations

Table 1. PdCuAu samples studied

Sample	Deposition time (min)			Thickness[a] (μm)
	Pd	Cu	Au	
$Pd_{71}Cu_{26}Au_3$	120	20	40	14
$Pd_{70}Cu_{25}Au_5$	120	20	40	14
$Pd_{67}Cu_{24}Au_9$	120	20	50	5
$Pd_{62}Cu_{36}Au_2$	120	30	30	14
$Pd_{60}Cu_{37}Au_3$	120	30	30	14

[a]Determined by the gravimetric method.

Colour online, B&W in print

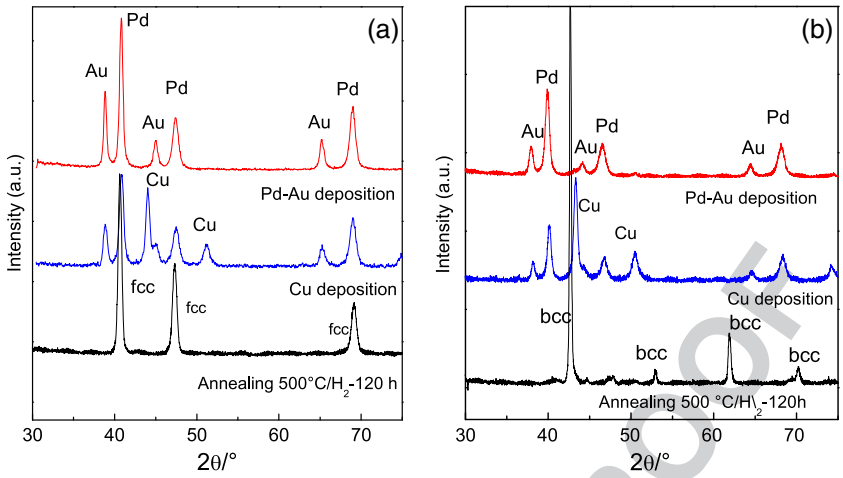

Figure 2. X-ray diffraction patterns of the as-synthesized PdCuAu ternary alloys and after annealing up to 500 °C during 120 h in hydrogen: (a) $Pd_{70}Cu_{26}Au_4$, (b) $Pd_{60}Cu_{37}Au_3$.

Table 2. Samples studied: atomic composition based on EDX measurements, crystal structure and lattice parameter determined by XRD

Sample composition (at%)	Phase	Lattice parameter (Å)	Reference
$Pd_{70}Cu_{26}Au_4$	fcc	3.90	[24]
$Pd_{66}Cu_{26}Au_9$	fcc	3.86	[25]
$Pd_{74}Cu_{19}Au_7$	fcc	3.87	[25]
$Pd_{45}Cu_{54}Au_1$	bcc	2.96	[25]
$Pd_{71}Cu_{26}Au_3$	fcc	3.85	This work
$Pd_{70}Cu_{25}Au_5$	fcc	3.84	This work
$Pd_{67}Cu_{24}Au_9$	fcc	3.84	This work
$Pd_{62}Cu_{36}Au_2$	bcc	2.99	This work
$Pd_{60}Cu_{37}Au_3$	bcc	3.00	This work

that were related to the variation in the film composition.[25] After annealing a $Pd_{35.6}Cu_{60.5}Au_{3.9}$ sample at 400 °C, Guerreiro *et al.*[25] reported an fcc to bcc phase transition. As stated previously, our alloys with a higher copper concentration ($Pd_{60}Cu_{37}Au_3$ and $Pd_{62}Cu_{36}Au_2$) yielded a bcc structure upon annealing at 500 °C.

The lattice parameter of the electroless-deposited PdCuAu samples determined from XRD data are summarized in Table 2. Lattice constants were determined from the positions of the fcc (111) and the bcc (110) diffraction features using the following relationship:

$$L = d_{hkl}\sqrt{h^2 + l^2 + k^2} \quad (2)$$

where d_{hkl} is the distance between two adjacent planes and L is the lattice parameter.

A change in the lattice parameter from 3.84 Å in the fcc phase to 2.99 Å for the bcc was observed for the PdCuAu samples studied in the present work; they are similar to the values reported by Guerreiro *et al.*[25] The PdCuAu data are also consistent with the PdCu binary alloy, for which the fcc to bcc phase transformation is accompanied by a reduction in the lattice parameter from ca. 3.76 to 2.97 Å.[26]

The morphologies of the PdCuAu electroless-deposited alloy samples were characterized by SEM. Figure 3 shows the SEM top-view images of the $Pd_{71}Cu_{26}Au_3$ and $Pd_{62}Cu_{36}Au_2$ samples after annealing at 500 °C for 120 h in hydrogen. All samples displayed a homogeneous morphology, displaying cauliflower-shaped clusters with well-defined borders. Sample $Pd_{62}Cu_{36}Au_2$ shows a smoother surface, with less-defined cluster borders, which could be attributed to the higher Cu content of this sample. The morphology of this sample is similar to that of PdCu samples synthesized by electroless deposition.[27] It should be noted that the SEM top view of the $Pd_{62}Cu_{36}Au_2$ shows pores in the surface, which could be caused by the Kirkendall effect as previously reported for PdCu membranes.[27] This effect occurs when two metals with different diffusion coefficients undergo inter-diffusion. EDX spot scans were performed at several points on the surface to determine the composition of the alloy. In all cases, the bulk composition determined by EDX revealed a uniform composition.

Surface analysis

XPS and LEIS spectroscopy were employed to determine the composition of the near-surface region and the top-most surface layer, respectively, of the PdCuAu samples under study. After the annealing, the PdCuAu samples were exposed to ambient conditions and transferred to the load-lock chamber of the spectrometer where the treatment in flowing H_2(5%)/Ar were performed. This treatment removes most of the oxygen present in the samples. From the curve fitting of the ~~Pd3p-O1s~~ region (not shown), it was possible to determine that all the samples contained a similar proportion of oxygen on the surface. The atomic concentration was 32 and 8% before and after treatment in flowing H_2(5%)/Ar, respectively. On the other hand, the carbon concentration was in all cases between 10 and 15% before and after treatment.

Because the XPS Pd $3d_{5/2}$ core-level peak is almost coincident with Au $4d_{5/2}$, the Pd $3d_{3/2}$ feature was used in the interpretation of the spectra. Table 3 shows the Pd $3d_{3/2}$ binding energies (BEs) of the PdCuAu ternary alloy samples studied in comparison with those of $Pd_{70}Cu_{30}$ (fcc), $Pd_{91}Au_9$ (fcc) and Pd reference samples. The BE of the Pd $3d_{3/2}$ peak for the PdCuAu samples displays a slight shift to lower energies (340.3 ± 0.1 eV) with respect to the pure Pd (340.5 ± 0.1 eV), which is likely related to the alloy formation (Table 3). In the same way, the Cu $2p_{3/2}$ photoemission feature exhibited a shift to lower BEs, which was assigned to the alloy formation in agreement with the data reported for binary and ternary PdCu alloys.[17,28] On the other hand, the Au $4f_{7/2}$ peaks in the PdCuAu ternary alloys did not show a significant shift upon alloying. However, in the PdAu system, a Pd $3d_{3/2}$ and Au $4f_{7/2}$ core-level shift was reported.[14] Hüfner *et al.*[29] reported a chemical shift of

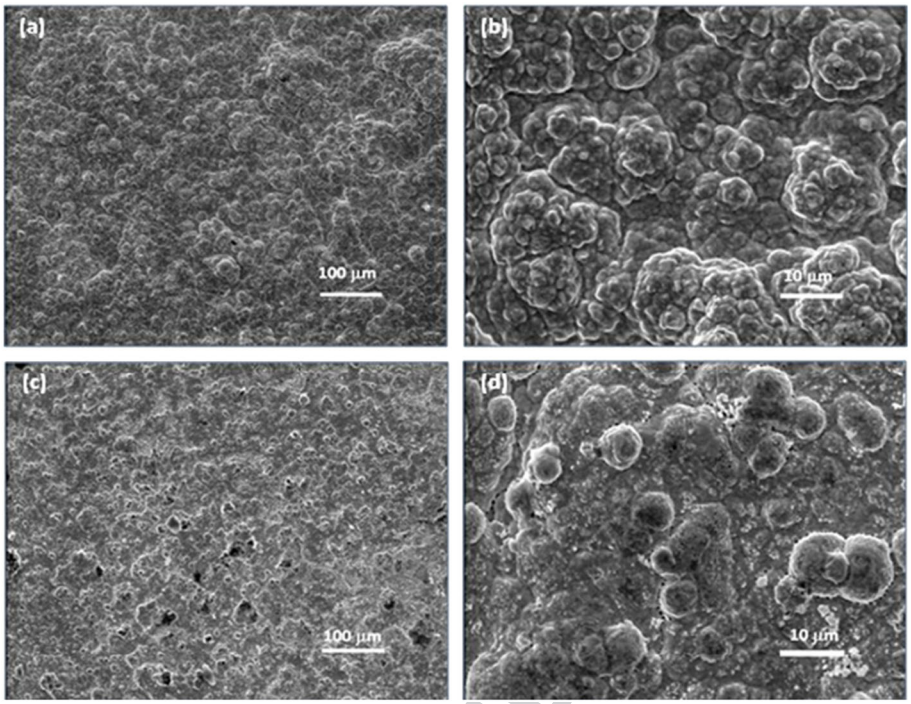

Figure 3. SEM top view of the $Pd_{71}Cu_{26}Au_3$ (a, b) and $Pd_{62}Cu_{36}Au_2$ (c, d) samples after annealing up to 500 °C in H_2 120 h at two different magnifications.

Table 3. XPS measurements of surface atomic composition, binding energy (BE) and full width at half maximum (fwhm) of the Pd $3d_{3/2}$, Cu $2p_{3/2}$ and Au $4f_{7/2}$ peaks for the PdCuAu ternary samples studied

Sample	Phase	BE ±0.1 (eV)			fhwm ±0.1 (eV)			Atomic composition			Line shape of the Pd $3d_{3/2}$ peak[d]
		Pd $3d_{3/2}$	Cu $2p_{3/2}$	Au $4f_{7/2}$	Pd $3d_{3/2}$	Cu $2p_{3/2}$	Au $4f_{7/2}$	Pd	Cu	Au	
$Pd_{70}Cu_{25}Au_5$	fcc	340.1	931.5	83.6	0.9	1.2	1.1	83	14	3	A(0.3,0.3,0)GL(30)
$Pd_{71}Cu_{26}Au_3$	fcc	340.3	931.6	83.8	1.1	1.1	1.2	75	22	3	A(0.3,0.3,0)GL(30)
$Pd_{60}Cu_{37}Au_3$	bcc	340.2	931.5	83.8	1.0	1.1	0.9	72	25	3	A(0.3,0.3,0)GL(30)
$Pd_{67}Cu_{24}Au_9$	fcc	340.3	931.7	83.7	1.1	1.0	1.1	83	13	4	A(0.3,0.3,0)GL(30)
$Pd_{70}Cu_{30}$[a]	fcc	340.4	932.3	—	1.0	1.2	—	—	—	—	A(0.2,0.2,0)GL(30)
$Pd_{91}Au_9$[b]	fcc	340.5	—	83.7	1.2	1.0	1.0	—	—	—	A(0.35,0.35,0)GL(30)
Pd[c]		340.5	—	—	1.2	—	—	—	—	—	A(0.35,0.35,0)GL(30)
Cu[c]		—	932.5	—	—	1.1	—	—	—	—	—
Au[c]		—	—	83.8	—	—	1.0	—	—	—	—

[a]From reference.[17]
[b]From reference.[19]
[c]Reference samples.
[d]A(a,b,n)GL(p) where a and b are parameters that allow changing the asymptotic form of the asymmetric tail.

0.7 eV to lower BEs with the $Pd_{90}Au_{10}$ alloy formation. Similarly, Goodman and coworkers[14] reported a shift to lower BE of 0.15 and 0.45 eV to Pd $3d_{3/2}$ and Au $4f_{7/2}$, respectively, upon annealing a $Pd_{50}Au_{50}$ sample at 527 °C. In a previously published work,[19] we observed a Au $4f_{7/2}$ core-level chemical shift to lower BE after hydrogen permeation for several $Pd_{91}Au_9$ membranes synthesized by electroless deposition. The discrepancy with the data obtained in the PdCuAu alloy could be related with the low gold content.

The Pd 3d feature for the PdCuAu ternary alloy exhibited a slight decrease in the peak asymmetry with respect to the pure Pd reference sample. The Gaussian/Lorentzian product GL(p) line shapes used to the curve fitting of the Pd 3d peaks were A(a,b,n)GL(p) where a and b are parameters that allow changing the asymptotic form of the asymmetric tail (Table 3). Note that parameters 'a' and 'b' decrease for the PdCuAu and PdCu alloys with respect to the pure Pd and PdAu samples. Similar changes in the Pd 3d peak asymmetry have been reported for other PdCu binary and ternary alloy systems and have been interpreted as evidence of alloy formation.[17,30] Hedman and coworkers[30] reported a decrease in the full width at half maximum (fwhm) of Pd $3d_{5/2}$ with the increase in Cu concentration in the PdCu system, which was attributed to the change of the local density of states in the Fermi level, in agreement with the shift in the Cu $2p_{3/2}$ peak. On the other hand, for the PdCuAu samples studied in the present work, the symmetry of the Cu $2p_{3/2}$ and Au $4f_{7/2}$ photoemission peaks remain unchanged.

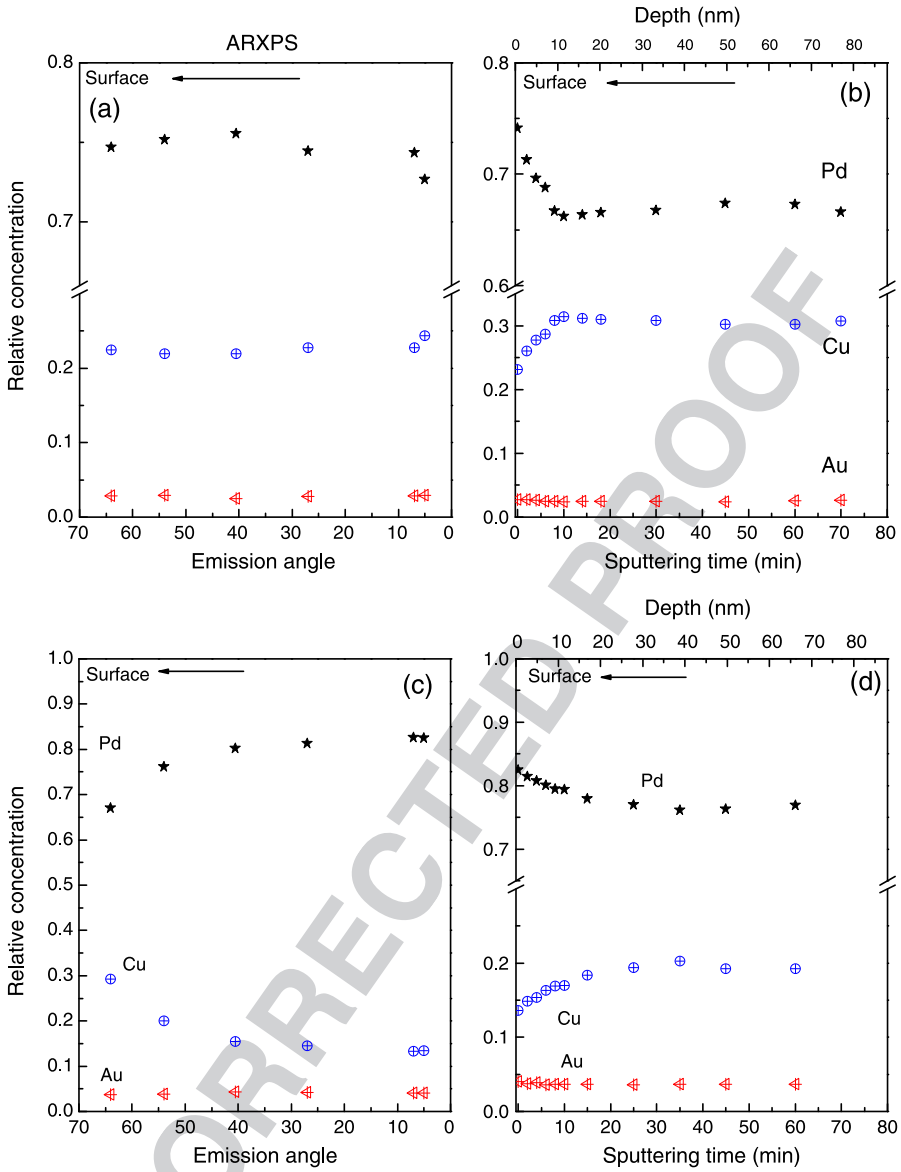

Figure 4. ARXPS and Ar^+-sputtering XPS depth profile for the $Pd_{62}Cu_{36}Au_2$ (a, b) and $Pd_{67}Cu_{24}Au_9$ (c, d) samples after annealing up to 500 °C.

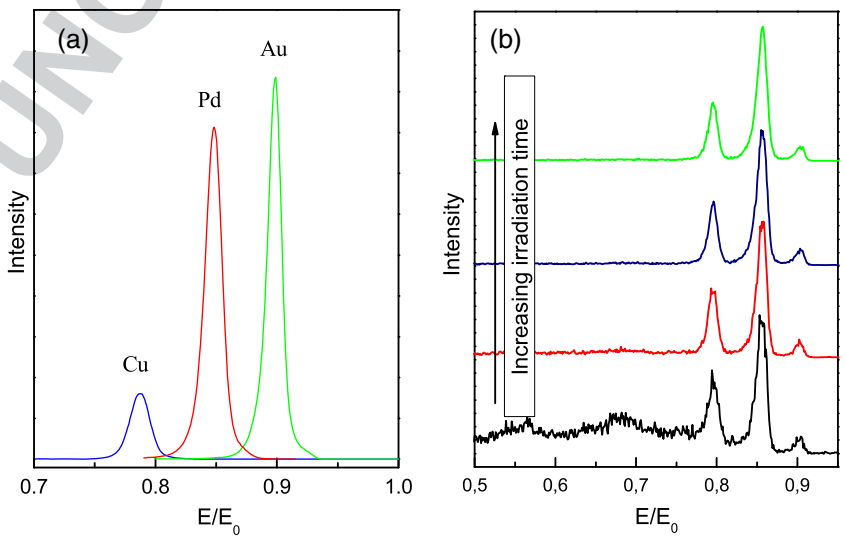

Figure 5. Characteristic LEIS spectra of the Pd, Cu and Au reference samples (a) and the $Pd_{71}Cu_{26}Au_3$ ternary alloy sample (b).

Taken together, the Pd $3d_{3/2}$ and Cu $2p_{3/2}$ chemical core-level shift and the Pd $3d_{3/2}$ fwhm changes observed here provide strong evidence for surface alloy formation, in agreement with the XRD data (Fig. 2).

It has been reported by Göthelid *et al.*[31] that the Doniach–Sunjic line profiles failed to describe the Pd 3d spectrum, specially to higher BE size as a result of changes in the density at the Fermi level. They mention that this apparent problem disappears upon adsorption because many adsorbates induce core-level shifts on that side of the spectrum. They studied the coverage dependence iodine structure on Pd (110). From curve fitting of the Pd $3d_{5/2}$ core level, they found the contribution of three components (the bulk and surface contributions and an extra component X) using a Gaussian–Lorentzian product and an asymmetric parameter.

Surface composition in the near-surface region and depth analysis

The near-surface atomic composition (ca. 6 atomic layers) of the samples was determined by XPS. As noted earlier, the Pd $3d_{5/2}$ signal is almost coincident with Au $4d_{5/2}$, so Pd $3d_{3/2}$ and Au $4f_{7/2}$ were used for quantification. Gaussian–Lorentzian product GL(p) line shapes modified by an asymmetric form were used for fitting the spectra. XPS wide-scan spectra revealed that, in addition to palladium, copper and gold, carbon and oxygen impurities were present. No signal from either Fe or Cr was detected; evidence that inter-diffusion between the component of the stainless steel support and the PdCuAu alloy had not occurred. All the PdCuAu samples displayed a slight Pd enrichment in the XPS-accessible near surface with respect to the bulk composition determined by EDX (Table 3).

Pd surface segregation under hydrogen atmosphere has been reported for the PdAg system. Shu *et al.*,[32] through XPS surface characterization of PdAg self-supported membranes, concluded that the chemisorption of hydrogen induces palladium surface segregation. In the same way, we have previously reported a higher Pd surface concentration in a PdAg sample after treatment in H_2(5%)/Ar at 400 °C, when it was compared with the sample without treatment.[33] For the ternary alloy samples studied in this work, a similar effect could be occurring.

To estimate the relative atomic distribution of the elements as a function of depth into the surface, both angle-resolved and Ar^+ sputter depth profiling, XPS measurements were performed. ARXPS experiments provide detailed information about composition within the XPS-accessible near surface of ca. 6 atom layers. Figures 4a and 4c summarize the ARXPS data obtained from the $Pd_{62}Cu_{36}Au_2$ (bcc phase) (Fig. 4a) and the $Pd_{67}Cu_{24}Au_9$ (fcc phase) (Fig. 4c) samples after annealing at 500 °C for 120 h. For the $Pd_{62}Cu_{36}Au_2$ sample, no major changes in the near-surface region composition were observed (Fig. 4a). On the other hand, for the $Pd_{67}Cu_{24}Au_9$ sample, the Cu concentration increased with increasing emission angle (more surface sensitive), while the Pd relative concentration decreased in the same way (Fig. 4c). These data suggest a Cu segregation to the top-most surface region for the fcc $Pd_{67}Cu_{24}Au_9$ alloy.

Additionally, in order to have an indication of the element distribution in a deeper region, Ar^+-sputtering XPS depth profiles were performed. The atomic compositions of the Pd, Cu and Au as a function of the etching time for the $Pd_{62}Cu_{36}Au_2$ (bcc) and $Pd_{67}Cu_{24}Au_9$ (fcc) samples are plotted in Fig. 4b and 4d, respectively; in both samples, the Pd atomic composition decreased with etching time while the Cu concentration increased. At larger depths, the Pd, Cu and Au concentration reached steady state, which are close to the bulk compositions measured by EDX. Note that the Ar^+-sputtering depth profile for $Pd_{67}Cu_{24}Au_9$ differed from the element distribution observed in the near-surface region (ARXPS) where Cu segregation to the top-most surface region was observed (Fig. 4c).

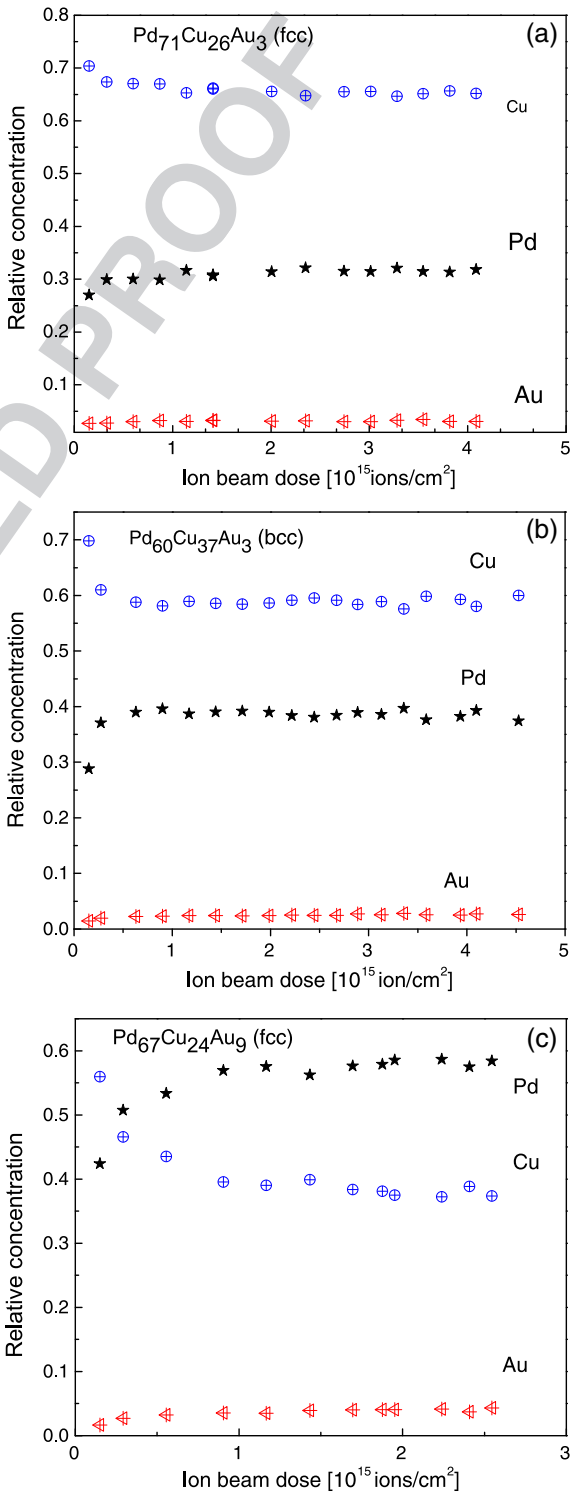

Figure 6. Pd, Cu and Au LEIS concentration as a function of the ion dose for the (a) fcc $Pd_{71}Cu_{26}Au_3$, (b) bcc $Pd_{60}Cu_{37}Au_3$ and (c) fcc $Pd_{67}Cu_{24}Au_9$ ternary alloy samples.

Top-most surface region characterization

To characterize the top-most atomic layer of the surface region, we performed LEIS analysis using 1 keV He^+ ions. As mentioned in the preceding texts, prior to the analysis, calibration of ion scattering signals was performed on pure palladium, copper and gold samples with a He^+ background pressure of 7×10^{-8} Torr, at room temperature. At the experimental conditions used in this work, no overlapping of the Pd, Cu and Au peaks was observed, which allowed us to perform a quantitative study. The characteristic normalized LEIS spectra taken at room temperature for the F5 $Pd_{71}Cu_{26}Au_3$ sample are shown in Fig. 5. The spectra exhibit three main peaks located at E_1/E_0 0.85, 0.79 and 0.90, which could be assigned to Pd, Cu and Au, respectively. The reference peaks of Pd, Cu and Au are shown for comparison. The measured values agree well with those obtained from the single collision model theoretical expression.[34] Two additional features assigned to Na ($E/E_0 = 0.55$) and K ($E/E_0 = 0.70$) appear in the first spectrum, which could be originated from the compounds used in the sample preparation by electroless deposition. The background observed in the first spectrum (Fig. 5) could be attributed to some gaseous surface contamination. Additionally, the intensity of the three peaks increases during the first seconds of ion beam irradiation as a consequence of the elimination of some gaseous surface contamination. A similar behavior has been reported for other systems.[35]

Using the experimentally determined sensitivity factors, the variation of Pd, Cu and Au composition as a function of the ion dose F6 was calculated using Eqn (1). Figure 6 shows the relative concentration as a function of the He^+ ion dose for $Pd_{71}Cu_{26}Au_3$ (fcc), $Pd_{60}Cu_{37}Au_3$ (bcc) and $Pd_{67}Cu_{24}Au_9$ (fcc) samples after annealing at 500 °C in H_2 stream for 120 h. The time dependence of the LEIS data likely provides evidence of a changing composition depth profile in the underlying layers as a result of sputtering effects. Note that in the three samples, the Pd concentration increases within the LEIS accessible near-surface region while the Cu concentration decreases, which is in agreement with the results of the ARXPS experiments of $Pd_{67}Cu_{24}Au_9$ (Fig. 4c). The relative composition of Pd, Cu and Au can change with time as a result of different sputtering yields of the elements. However, the LEIS experiments suggest, in agreement with the ARXPS data, that Cu segregation to the top-most surface layer takes place upon annealing at 500 °C for 120 h. Note that the extent of segregation for the $Pd_{60}Cu_{37}Au_3$ sample was lower than the observed for the $Pd_{67}Cu_{24}Au_9$ sample. This could be one of the reasons why in the ARXPS data of the $Pd_{62}Cu_{36}Au_2$ sample, no major change in the Pd, Cu and Au composition was observed as a function of takeoff angle. The small differences observed among the samples appear to be related to the higher gold concentration on the $Pd_{67}Cu_{24}Au_9$ rather than to the alloy structure (fcc or bcc). Another factor that should be considered is the surface roughness as well as the morphology of the films, because the angular variation of the XPS peak intensity depends on the surface roughness.[36]

The bulk (EDX), near-surface (XPS) and top-most surface (LEIS) Pd and Cu compositions of the PdCuAu alloy samples are compared in Fig. 7. For all samples, Pd composition of the near-surface region is F7 above the bulk composition, the Pd content in the top-most surface region is below that of both the bulk and the near surface. This pattern could be related to migration of Cu from the atomic layers immediately below the top layer to the top layer, as reported for other alloy systems.[7] In contrast with the Pd and Cu behavior, the Au composition of the PdCuAu ternary alloys determined by XPS and LEIS did not show a significant difference with respect to the bulk composition.

The segregation behavior observed in the PdCuAu system is different from that reported for the PdCuAg alloys, where a cosegregation of Cu and Ag in the near-surface region and Ag enrichment to the top-most surface layer takes place.[17] This is likely related to a different interaction of the minority component, Au for the PdCuAu system and Ag for the PdCuAg alloy, with the parent PdCu binary. The surface segregation in the PdCu alloy system has been previously studied on both single and polycrystalline crystals.[7,8] Surface studies have shown that the top atomic layer of PdCu alloys is rich in Cu, whereas the near-surface region (~7 atomic layers) is rich in Pd, as reported by Miller *et al.*[7] These data were consistent with those reported by Loboda-Cackovic *et al.*[8] using AES and TPD of CO. For the CuAu binary system, a weak segregation of gold to the surface has been reported.[37] This behavior is driven by the lower surface energy of Au in relation to that of Cu and to the larger size of the Au atom. Nevertheless, for the CuAuAg ternary alloys, the surface concentration of Au is strongly suppressed at the surface when it is compared with that of the CuAu binary alloy.[16]

The data presented in this work suggest that the PdCuAu alloys could be promising materials to be applied as membranes for hydrogen purification. The presence of excess Cu atoms at the top surface, where H_2S first interacts with the alloy, may contribute to the alloy's resistance to corrosion. We tested the hydrogen

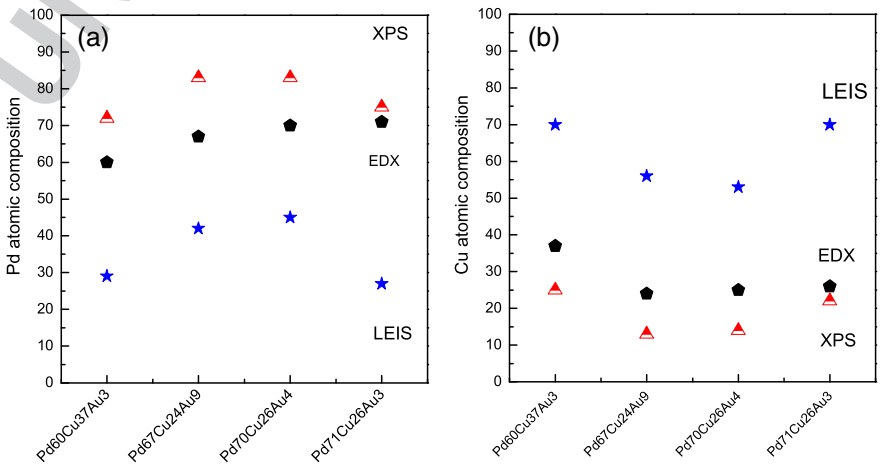

Figure 7. LEIS, XPS and EDX composition of the PdCuAu samples studied. (a) Pd at% and (b) Cu at%.

Table 4. Permeation data of the PdCuAu alloy compared with pure Pd, PdAu and PdCu and reported data

Sample	Phase	Thickness (μm)	Permeability (mol s^{-1} m^{-1} $Pa^{-0.5}$)	Temperature (°C)	Reference
$Pd_{60}Cu_{37}Au_3$	bcc	14	2.9×10^{-9a}	400	[38]
$Pd_{70}Cu_{25}Au_5$	fcc	14	1.9×10^{-9a}	400	[38]
$Pd_{91}Au_9$	fcc	12	9.9×10^{-9a}	400	[40]
$Pd_{67}Cu_{33}$	fcc	26	1.3×10^{-9a}	400	[20]
Pd	fcc	14	1.2×10^{-8a}	400	[40]
$Pd_{72}Cu_{26}Au_2$	fcc	10	3.0×10^{-9a}	400	[39]
$Pd_{56}Cu_{41}Au_3$	fcc	10	1.5×10^{-9a}	400	[39]
$Pd_{71.5}Cu_{27}Au_{1.5}$	fcc	2.1	4.2×10^{-9b}	400	[39]

[a]Feed: pure hydrogen.
[b]Feed: 90% H_2/N_2, Ar sweep gas, temperature = 400 °C

permeability and H_2S tolerance of selected PdCuAu ternary alloy membranes synthesized on top of porous stainless steel disks.[38] Upon exposure to 100 ppm H_2S/H_2 at 400 °C for 24 h, all PdCuAu membranes experienced flux reductions of ~55%, followed by recovery to ~80% of the initial hydrogen flux upon reintroduction of pure hydrogen at 400 °C. In agreement with the XRD results, sulfur was not detected in the bulk of H_2S-exposed PdCuAu samples by EDS. A summary of our results[38] compared with those reported in the literature is presented in Table 4. Note that our results are consistent with the previous reports. We observed that the introduction of gold to the PdCu binary improves hydrogen permeation, in agreement with the data previously reported for magnetron-sputtered samples.[24,39] Peters *et al.*[39] reported a slight increase in permeability compared with the binary alloy for the PdCuAu system with a composition of about $Pd_{71.5}Cu_{27}Au_{1.5}$ ($4.2\ 10^{-9}$ mol s^{-1} m^{-1} $Pa^{-0.5}$) when the sample was exposed to a 90% H_2/N_2 mixture using Ar as sweep gas.

Conclusions

PdCuAu ternary alloys with composition that display high resistance to H_2S corrosion were synthesized by the sequential electroless deposition technique on top of ZrO_2-modified porous stainless steel disks. The method delivered homogeneous, continuous, defect-free films as revealed by SEM-EDX. After annealing at 500 °C for 120 h in hydrogen, a fcc structure was obtained for the $Pd_{70}Cu_{26}Au_4$, $Pd_{71}Cu_{26}Au_3$ and $Pd_{67}Cu_{24}Au_9$ samples and a bcc phase for $Pd_{60}Cu_{37}Au_3$ and $Pd_{62}Cu_{36}Au_2$, as evidenced by XRD.

The surface alloy formation was confirmed by XPS, where a core-level chemical shift of the Pd $3d_{3/2}$ and the Cu $2p_{3/2}$ features, together with the changes in the fwhm of the Pd $3d_{3/2}$ peak, were observed.

The near-surface region characterized by XPS became enriched in Pd with respect to the bulk composition determined by EDX. In contrast, the top-most surface layer composition was in all samples copper-rich compared with the bulk composition as revealed by LEIS. This high Cu concentration could contribute to resistance to bulk sulfide formation in the PdCuAu alloy membranes.

Acknowledgements

The authors wish to acknowledge the financial support received from UNL, CONICET and ANPCyT. They are also grateful to ANPCyT for Grant PME 8-2003 to finance the purchase of the UHV Multi-Analysis System. Thanks are given to Elsa Grimaldi for the English language editing.

References

[1] F. A. Lewis, *Platinum Met. Rev.* **1996**, *40*, 180–187.
[2] J.K. Ali, E.J. Newson, D.W.T. Rippin, *J. Membr. Sci.* **1994**, *89* 171–184.
[3] Ø. Hatlevik, S. K. Gade, M. K. Keeling, P. M. Thoen, A.P. Davidson, J. Douglas Way, *Sep. Purif. Technol.* **2010**, *73*, 59–64.
[4] B.D. Morreale, M.V. Ciocco, B.H. Howard, R.P. Killmeyer, A.V. Cugini, R. M. Enick, *J. Membr. Sci.* **2004**, *241*, 219–224.
[5] C-H. Chen, Y. H. Ma, *J. Membr. Sci.* **2010**, *362* 535–544.
[6] F. Roa, J. Douglas Way, *Ind. Eng. Chem. Res.* **2003**, *42* (23) 5827–5835.
[7] J. B. Miller, Ch. Matranga, A. J. Gellman, *Surf. Sci.* **2008**, *602* 375–382.
[8] J. Loboda-Cackovic, M.S. Mousa, J.H. Block, *Vacuum* **1995**, *46* 89–96.
[9] R.H. Bergmans, M. van de Grift, A.W. Denier van der Gon, H. H. Brongersma, *Surf. Sci.* **1996**, *345*, 303–312.
[10] P. Deurinck, C. Creemers, *Surf. Sci.* **1998**, *419*, 62–77.
[11] R. Beikler, E. Taglauer, *Nucl. Instr. and Meth. B* **2002**, *193*, 455–459.
[12] J. Tersoff, *Phys. Rev. B* **1990**, *42*, 10965–10968.
[13] L. Piccolo, A. Piednoir, J-C. Bertolini, *Surf. Sci.* **2005**, *592*, 169–181.
[14] C.-W. Yi, K. Luo, T. Wei, D. W. Goodman, *J. Phys. Chem. B* **2005**, *109*, 18535–18540.
[15] P. Gargano, H. Mosca, G. Bozzolo, *Phys. B* **2009**, *404*, 2769–2772.
[16] M. A. Hoffman, P. Wynblatt, *Metall. Trans. A* **1991**, *22A* 1833–1840.
[17] A. M. Tarditi, L. M. Cornaglia, *Surf. Sci.* **2011**, *605*, 62–71.
[18] B. Fleutot, J. B. Miller, A. J. Gellman, *J. Vac. Sci. Technol. A.* **2012**, *30*, 061511–061521
[19] A.M. Tarditi, C. Gerboni, L. Cornaglia, *J. Membr. Sci.* **2013**, *428*, 110.
[20] A. M. Tarditi, F. Braun, L. M. Cornaglia, *Appl. Surf. Sci.* **2011**, *257*, 6626–6635.
[21] S. Hofmann, *Depth profiling in AES and XPS, D. Briggs, MP, Seah, Practical surface analysis, Auger and X-ray photoelectron spectroscopy*. Wiley, New York, **1990** 143–255.
[22] P.R. Subramanian, D.E. Laughlin *J Phase Equilibr.* **1991**, *12*, 231–236.
[23] T.A. Peters, T. Kaleta, M. Stange, R. Bredesen, *J. Membr. Sci.* **2011**, *383*, 124– 134.
[24] K. E. Coulter, J. D. Way, S.K. Gade, S. Ch. Chaudhary, D. S. Sholl, L. Semidy-Flecha, *J. Phys. Chem. C* **2010**, *114*, 17173–17180.
[25] B. H. Guerreiro, m. H. Martin, L. Roué, D. Guay, *Int. J. Hydrogen Energy* **2014**, *39*, 3487–3497.
[26] N. Pomerantz, Y.H. Ma, *Ind. Eng. Chem. Res.* **2009**, *48*, 4030–4039.
[27] N. Pomerantz, Y. H. Ma, E. A. Payzant, *AIChE J.* **2010**, *56*, 3062–3073.
[28] H. Gao, J.Y. S. Lin, Y. Li, B. Zhang, *J. Membr. Sci.* **2005**, *265*, 142–152.
[29] S. Hüfner, G.K. Wertheim, J.H. Wernick, *Solid State Commun.* **1975**, *17*, 417–422.
[30] N. Martenson, R. Nyholm, H. Calén, J. Hedman, *Phys. Rev. B.* **1981**, *24* (4) 1725–1735.
[31] M. Göthelid, M. Tymczenko, W. Chow, S. Ahmadi, S. Yu, B. Bruhn, D. Stoltz, H. von Schenck, J. Weissenrieder, Ch. Sun, *J. Chem. Phys.* **2012**, *137*, 204703.
[32] J. Shu, A. Adnot, B. P. A. Grandjean, S. Kaliaguine, *Thin Solid Films* **1996**, *286*, 72–79.
[33] A. Tarditi, M. L. Bosko, L. M. Cornaglia, *Int. J. Hydrogen Energy* **2012**, *37*, 6020–6029.

[34] H. Niehus, W. Heiland, E. Taglauer, *Surf. Sci. Reports* **1993**, *17*, 213–303.
[35] P. Delichère, K.E. Béré, M. Abon, *Appl. Catal. Gen.* **1998**, *172*, 295–309.
[36] A. I. Martín-Concepción, F. Yubero, J. P. Espinós, S. Tougaard, *Surf. Interface Anal.* **2004**, *36*, 788–792.
[37] M.A. Hoffmann, P. Wynblatt, *Surf. Sci.* **1990**, *236*, 369–376.
[38] A. M. Tarditi, Carolina Imhoff, Fernando Braun, James Miller, Andrew Gellman, Laura Cornaglia, *J. Membr. Sci.* **2015**, *479*, 246–255.
[39] T.A. Peters, T. Kaleta, M. Stange, R. Bredesen, *J. Membr. Sci.* **2013**, *429*, 448–458.
[40] F. Braun, A. M. Tarditi, J. B. Miller, L. M. Cornaglia, *J. Membr. Sci.* **2014**, *450*, 299–307.

Author Query Form

Journal: Surface and Interface Analysis

Article: sia_5759

Dear Author,

During the copyediting of your paper, the following queries arose. Please respond to these by annotating your proofs with the necessary changes/additions.

- If you intend to annotate your proof electronically, please refer to the E-annotation guidelines.
- If you intend to annotate your proof by means of hard-copy mark-up, please use the standard proofing marks. If manually writing corrections on your proof and returning it by fax, do not write too close to the edge of the paper. Please remember that illegible mark-ups may delay publication.

Whether you opt for hard-copy or electronic annotation of your proofs, we recommend that you provide additional clarification of answers to queries by entering your answers on the query sheet, in addition to the text mark-up.

Query No.	Query	Remark
Q1	AUTHOR: "Physical vapor deposition" was provided as the definition for "PVD". Please check and change as necessary.	OK
Q2	AUTHOR: "Deionized" was provided as the definition for "DI". Please check and change as necessary.	OK
Q3	AUTHOR: Figures 1, 2, and 4–7 have been supplied in colour. Academic authors receive one page of colour in print free of charge where colour is justified to the journal editor. There is a charge of £350 for the second page and £150 per page for pages 2, 4 and 6–8. Additional colour costs available on application. Industrial and government authors do not receive free colour. Please confirm if this figure is to be reproduced in (a) colour in print, (b) colour online only (at no charge to author) or (c) black and white. Colour will be invoiced when article is published in print. Also please note that for the option "(b) colour online only (at no charge to author)" could you kindly identify and make necessary text amendments that may need to be made in the caption or text with regard to this change.	Colour online only
Q4	AUTHOR: Please check equations, and any associated equation citations in the main text, have been reordered/renumbered correctly.	OK

WILEY

USING e-ANNOTATION TOOLS FOR ELECTRONIC PROOF CORRECTION

Required software to e-Annotate PDFs: Adobe Acrobat Professional or Adobe Reader (version 7.0 or above). (Note that this document uses screenshots from Adobe Reader X)
The latest version of Acrobat Reader can be downloaded for free at: http://get.adobe.com/uk/reader/

Once you have Acrobat Reader open on your computer, click on the Comment tab at the right of the toolbar:

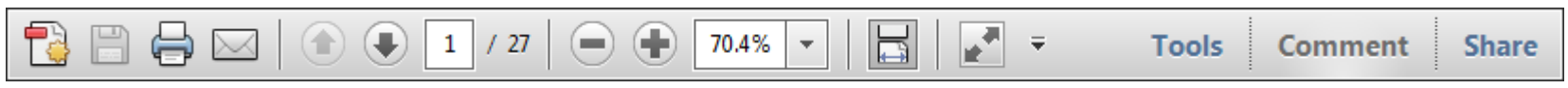

This will open up a panel down the right side of the document. The majority of tools you will use for annotating your proof will be in the Annotations section, pictured opposite. We've picked out some of these tools below:

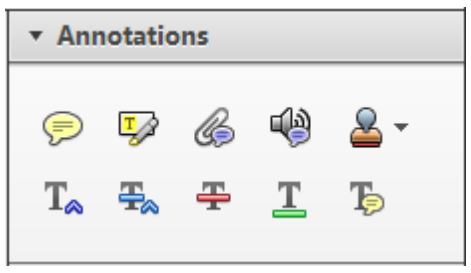

1. Replace (Ins) Tool – for replacing text.

Strikes a line through text and opens up a text box where replacement text can be entered.

How to use it

- Highlight a word or sentence.
- Click on the Replace (Ins) icon in the Annotations section.
- Type the replacement text into the blue box that appears.

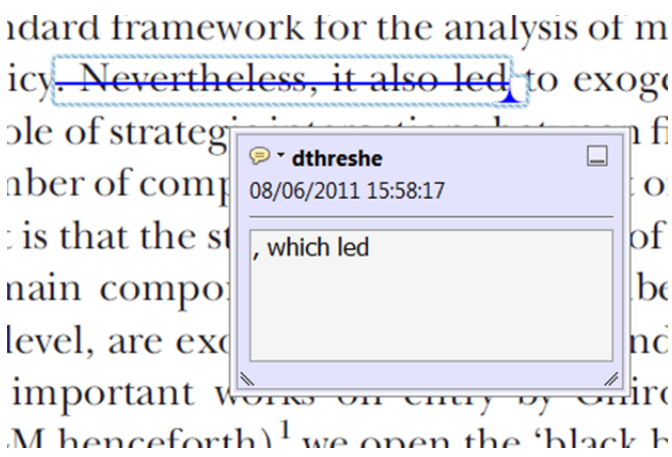

2. Strikethrough (Del) Tool – for deleting text.

Strikes a red line through text that is to be deleted.

How to use it

- Highlight a word or sentence.
- Click on the Strikethrough (Del) icon in the Annotations section.

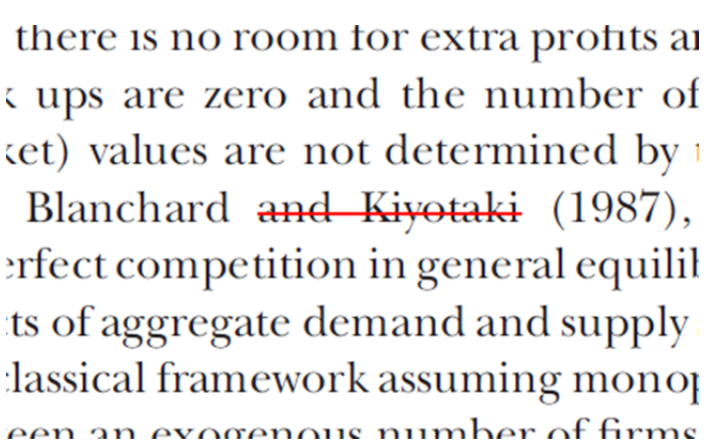

3. Add note to text Tool – for highlighting a section to be changed to bold or italic.

Highlights text in yellow and opens up a text box where comments can be entered.

How to use it

- Highlight the relevant section of text.
- Click on the Add note to text icon in the Annotations section.
- Type instruction on what should be changed regarding the text into the yellow box that appears.

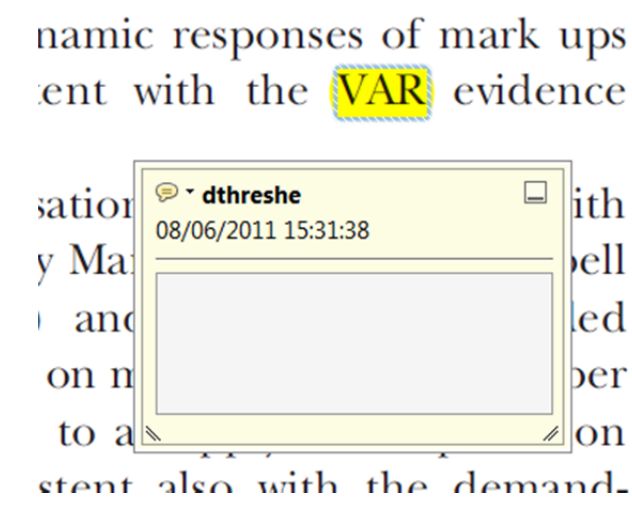

4. Add sticky note Tool – for making notes at specific points in the text.

Marks a point in the proof where a comment needs to be highlighted.

How to use it

- Click on the Add sticky note icon in the Annotations section.
- Click at the point in the proof where the comment should be inserted.
- Type the comment into the yellow box that appears.

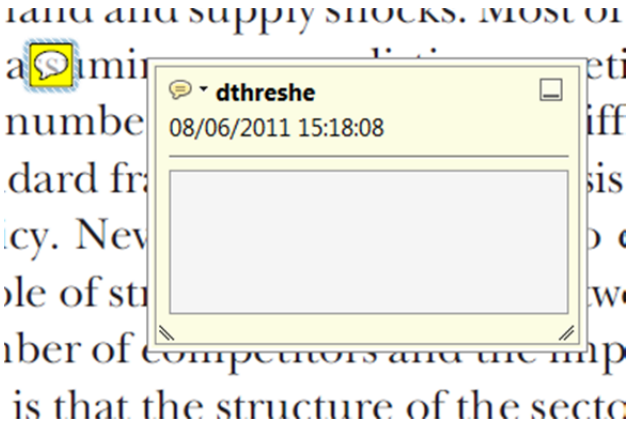

WILEY

USING e-ANNOTATION TOOLS FOR ELECTRONIC PROOF CORRECTION

5. Attach File Tool – for inserting large amounts of text or replacement figures.

Inserts an icon linking to the attached file in the appropriate pace in the text.

How to use it

- Click on the Attach File icon in the Annotations section.
- Click on the proof to where you'd like the attached file to be linked.
- Select the file to be attached from your computer or network.
- Select the colour and type of icon that will appear in the proof. Click OK.

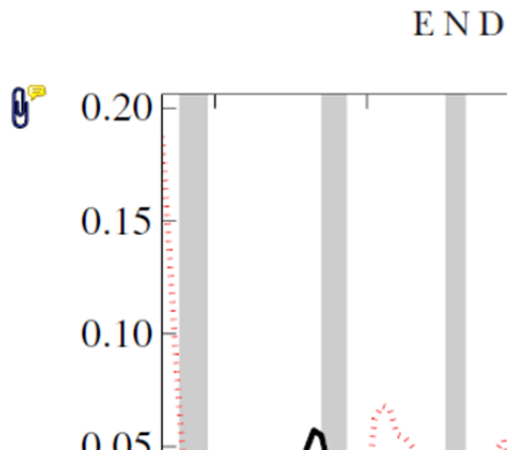

6. Add stamp Tool – for approving a proof if no corrections are required.

Inserts a selected stamp onto an appropriate place in the proof.

How to use it

- Click on the Add stamp icon in the Annotations section.
- Select the stamp you want to use. (The Approved stamp is usually available directly in the menu that appears).
- Click on the proof where you'd like the stamp to appear. (Where a proof is to be approved as it is, this would normally be on the first page).

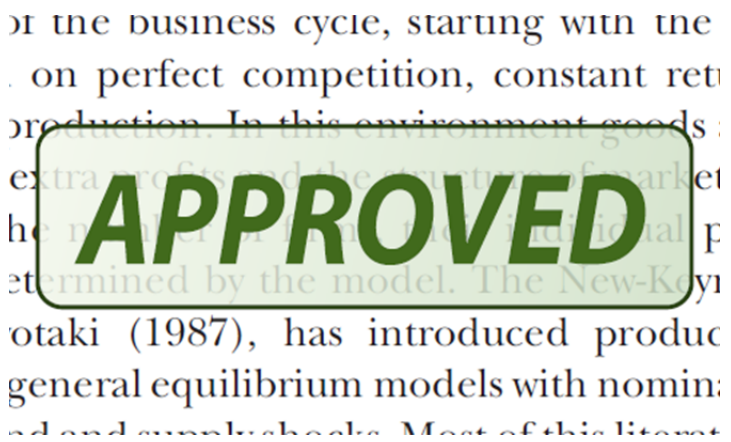

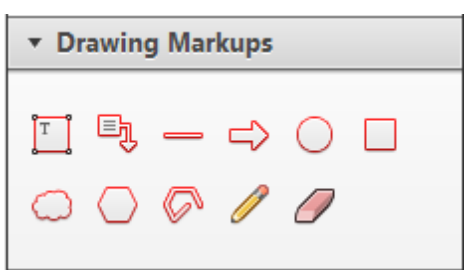

7. Drawing Markups Tools – for drawing shapes, lines and freeform annotations on proofs and commenting on these marks.

Allows shapes, lines and freeform annotations to be drawn on proofs and for comment to be made on these marks..

How to use it

- Click on one of the shapes in the Drawing Markups section.
- Click on the proof at the relevant point and draw the selected shape with the cursor.
- To add a comment to the drawn shape, move the cursor over the shape until an arrowhead appears.
- Double click on the shape and type any text in the red box that appears.

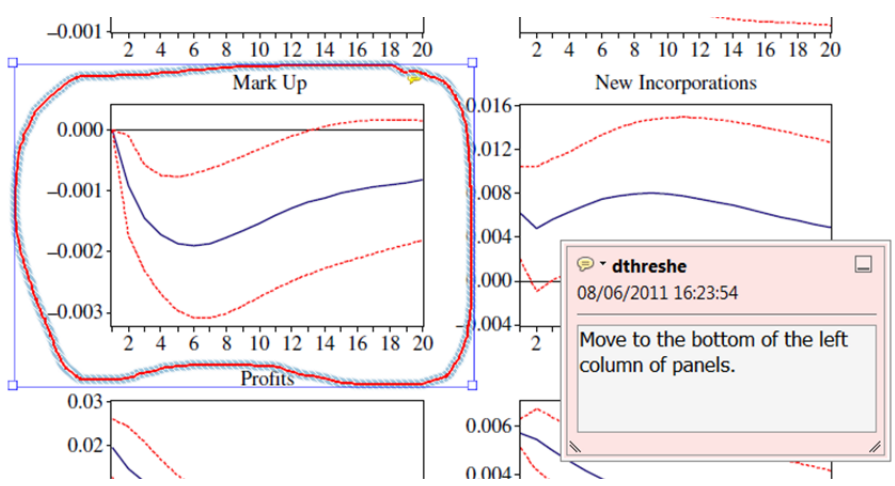

For further information on how to annotate proofs, click on the Help menu to reveal a list of further options: